# Three-phase soft-switching inverter for induction motor drives

K.H.Chao and C.M.Liaw

**Abstract:** A zero-voltage transition (ZVT) soft-switching inverter for an induction motor drive is developed. The proposed soft-switching inverter is formed from the traditional pulse-width modulated (PWM) inverter by simply augmenting with auxiliary resonant circuits, and the soft switching is achieved through applying PWM switching control signals with suitable delays for the main and auxiliary switches. No additional voltage and current sensors are required in the implementation. The operations and governing equations in various modes of the proposed soft-switching inverter are first analysed then, accordingly, a quantitative design procedure is given to find the values of the auxiliary resonant circuit components and the delay times of the switches for achieving ZVT control. Finally, the designed soft-switching inverter is used for powering an indirect field-oriented (IFO) induction motor drive to test its effectiveness. The simulation and measured results show that a smaller switching loss and higher conversion efficiency are obtained by the proposed soft-switching inverter.

## List of symbols

$C_{Ar+}$–$C_{Cr-}$, $C_r$ = sum of parasitic capacitance and added external capacitance of the main switches $T_{A+}$, $T_{A-}$, $T_{B+}$, $T_{B-}$, $T_{C+}$ and $T_{C-}$
$C_{ar+}$–$C_{cr-}$ = parasitic capacitances of $T_{Ar+}$, $T_{Ar-}$, $T_{Br+}$, $T_{Br-}$, $T_{Cr+}$ and $T_{Cr-}$
$C_{DAr+}$–$C_{DCr-}$ = parasitic capacitances of $D_{Ar+}$, $D_{Ar-}$, $D_{Br+}$, $D_{Br-}$, $D_{Cr+}$ and $D_{Cr-}$
$C_i$ = input filter capacitance of inverter
$D_{A+}$–$D_{C-}$ = anti-parallel diodes of main switches
$D_{Ar+}$–$D_{Cr-}$ = diodes used in auxiliary resonant branches for releasing the energy stored in the resonant inductor
$D_{ar+}$–$D_{ar-}$ = diodes used in auxiliary resonant branches to prevent the undesired resonance
$f_s$ = switching frequency of inverter
$I_D$ = continuous drain current of MOSFET
$I_{DM}$ = pulsed drain current of MOSFET
$i_{A+}$, $i_{A-}$ = currents of main switches $T_{A+}$ and $T_{A-}$
$I_{Ar+}$, $I_{Ar-}$ = currents of auxiliary switches $T_{Ar+}$ and $T_{Ar-}$
$I_{LAT}$ = resonant inductor current of auxiliary resonant branch of soft-switching inverter
$I_A$ = line current of induction motor
$I_{A,max}$ = maximum value of $I_A$
$I_A^*$ = current command of $I_A$
$i_{LAr,max}$ = maximum current of $i_{LAr}$
$i_{LAr,on}$ = resonant inductor current in on-state mode
$(i_{LAr,on})_{max}$ = maximum current of $I_{LAr,on}$
$L_{Ar}$, $L_{Br}$, $L_{Cr}$, $L_r$ = resonant inductors used in auxiliary resonant branch
$P_{A+}$, $P_{A-}$ = switching losses of $T_{A+}$ and $T_{A-}$
$P_{a+}$, $P_{a-}$ = switching losses of $T_{Ar+}$ and $T_{Ar-}$
$P_{out}$ = output power of inverter
$R_{DS(on)}$ = static drain-source on-state resistance of MOSFET
$R_{\theta JC}$ = junction-to-case thermal resistance of MOSFET
$T_{A+}$–$T_{C-}$ = main switches
$T_{Ar+}$–$T_{Cr-}$ = auxiliary switches
$T_j$ = maximum junction temperature of MOSFET
$T_s$ = switching period
$t_d$ = delay time for turning on the main switch
$t_\Delta$ = blanking time interval
$t_\varepsilon$ = small time interval greater than the forward recovery time of diode
$V_d$ = DC-link voltage of inverter
$V_{d,max}$ = maximum value of DC link voltage
$v_{A+}$, $v_{A-}$ = voltages across $T_{A+}$ and $T_{A-}$
$v_{a+}$, $v_{a-}$ = voltages across $T_{Ar+}$ and $T_{Ar-}$
$\omega_r$ = rotor angular speed

## 1 Introduction

It is known that the performance of a pulse-width modulated (PWM) inverter-fed system can be much improved by increasing the switching frequency. However, this will suffer by giving high switching losses and large switching stresses of the power devices, and moreover, the problem of electromagnetic interference [1, 2]. During the past decades, many attempts [3–12] have been made to solve these contradictory problems. Among these, the resonant DC-link inverter [3, 4] is the most commonly used one for induction



*IEE Proceedings* online no. 20010123

*DOI:* 10.1049/ip-epa:20010123

Paper first received 20th January and in revised form 17th May 2000

The authors are with the Department of Electrical Engineering, National Tsing Hua University, Hsinchu, Taiwan, Republic of China

motor drives, owing to its simplicity, but it possesses the disadvantage of having a high resonant link voltage, which is equal to or greater than twice the supply voltage. Several approaches [5, 6] have been developed to limit this overvoltage, but they are not suitable for performing PWM switching operations. In the existing parallel resonant DC-link circuit [7] and synchronised resonant DC-link converter [8], the soft switching is achieved using additional switches. Their resonant circuits are complex and difficult to control. In addition, their peak DC-link voltages are also higher than the supply voltage, and the auxiliary switch current is not zero during the steady-state, which will lead to increased conduction losses.

To solve the aforementioned overvoltage and the limitation of PWM operation problems, some resonant snubber-based soft-switching PWM inverters have been devised in [9–16]. Although the soft switching of main switches can easily be accomplished by adding auxiliary switching branches to the conventional inverter circuit and giving proper switching control signals, different problems still exist in different types of inverters. For example, the ordinary resonant snubber inverter [9] or the auxiliary resonant commutated pole inverter [10] needs two equal and bulky capacitors connected in series to accomplish commutation. The resonant zero-voltage transition (ZVT) inverters developed in [11, 12] require multiple transitions to achieve the desired state changes, and voltage clamping diodes are also needed to avoid overvoltage across the auxiliary resonant switch during resonant current resetting. Recently, a three-phase delta configured resonant snubber inverter for an induction motor drive has been developed [13]. The auxiliary resonant branches are connected between different phase-leg outputs to avoid using additional bulky capacitors and generating overvoltage in the resonant switches. However, it possesses a limitation in switching control as the nonadjacent state-space vector modulation is used for releasing the energy stored in the resonant inductor to accomplish soft switching. This limits the switching control flexibility and thus produces larger current ripples. In addition, its switching control signal generation scheme is still complicated.

A three-phase ZVT soft-switching inverter for an induction motor drive is developed in this paper. The proposed inverter circuit is formed from the conventional inverter with its main switches being connected in parallel with auxiliary resonant branches. The soft switching is successfully achieved by simply applying suitably modified switching control signals for the main and auxiliary switches during the blanking time periods of the original PWM signals. Since ZVS and/or ZCS at turn-on and turn-off of all main switches and diodes can be achieved, the switching losses can be significantly reduced. Compared with the main switch, the current rating of the auxiliary switch can be chosen to be much smaller owing to its very small conduction duty ratio. In addition, the overvoltage across the auxiliary resonant switch is also limited to be small by the proposed soft-switching scheme. Moreover, since the main switch and the auxiliary switch can be independently controlled, the PWM switching control of the inverter is very flexible. After performing the detailed analyses for all operation modes of the proposed inverter, a procedure is established to quantitatively design the circuit components. The validity of the designed inverter is verified by some simulation and experimental results on a vector-controlled induction motor drive with impressed currents [17, 18].

## 2 Operation principle and governed equations of the proposed soft-switching inverter

The system configuration of the proposed soft-switching inverter-fed induction motor drive is shown in Fig. 1. The power circuit and switching control mechanism of this soft-switching inverter are constructed from those of a conventional PWM inverter by only slight modifications. The switching signals generated from the conventional indirect field-oriented current-controlled PWM mechanism are processed by the proposed soft-switching control signal generating scheme to yield the desired switching signals. Fig. 2 shows the circuit configuration of the proposed three-phase soft-switching inverter. Each main switch leg is connected to an auxiliary switch leg through an inductor, which is common for the upper and lower parts of each leg. Each auxiliary resonant branch ($T_{A+}$ as an example) consists of an unidirectional auxiliary switch $T_{Ar+}$, two diodes $D_{Ar+}$ and $D_{ar+}$, a resonant inductor $L_{Ar}$ and a snubber capacitor $C_{Ar+}$ of the main switch $T_{A+}$. The diode $D_{Ar+}$ is used to provide a path for releasing the energy stored in $L_{Ar}$, and the diode $D_{ar+}$ is employed to prevent undesired resonance forming by the resonant inductor and the parasitic capacitor of the auxiliary switch.

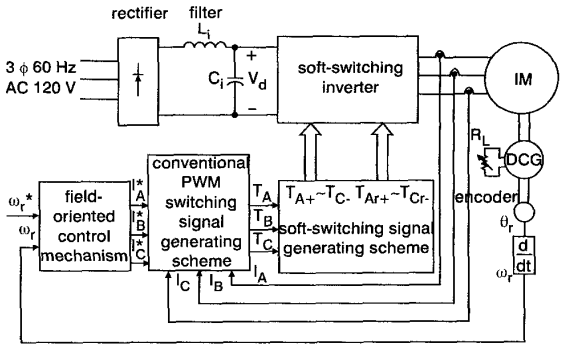


**Fig. 1** *System configuration of the proposed soft-switching inverter-fed indirect field-oriented induction motor drive*

The switching control signals of all switches during one particular switching period are shown in Fig. 3. The soft-switching of a main switch is achieved by the switching control of an auxiliary switch, whose turn-on period is allocated during the blanking time period of the main switch. Therefore the auxiliary switches only conduct in a very short time interval. Since each main switch of the proposed inverter can be independently operated, the analysis of the three-phase inverter switching operation can be made based on the single-phase approach. The operating principle of the proposed soft-switching inverter is explained by the turn-on and turn-off of the switches in leg A with the related voltage and current waveforms being sketched in Fig. 3.

To simplify the analysis, the following assumptions are made: the input filter capacitor $C_i$ is large enough so that the DC voltage $V_d$ can be assumed to be constant; all the resonant inductors and resonant capacitors are ideal and identical, i.e. $L_{Ar} = L_{Br} = L_{Cr} \triangleq L_r$ and $C_{Ar+} = C_{Ar-} = C_{Br+} = C_{Br-} = C_{Cr+} = C_{Cr-} \triangleq C_r$, where $C_r$ is the sum of the IGBT's parasitic capacitance and the added external capacitance, respectively, and the resonant inductance $L_r$ is much smaller than the motor inductance so that the load current can be regarded as constant during the short switching period. For the inverter with a lagging power factor load, as the main switch is turned on, it will be operated in an

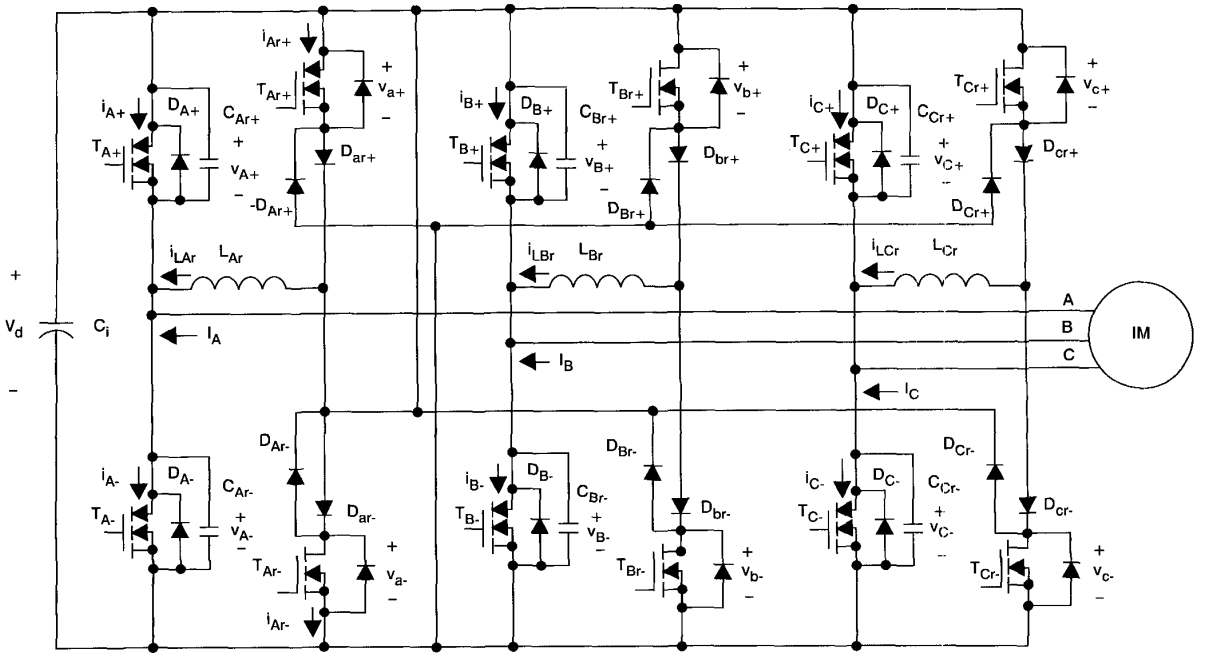


**Fig. 2** *The proposed three-phase soft-switching inverter*

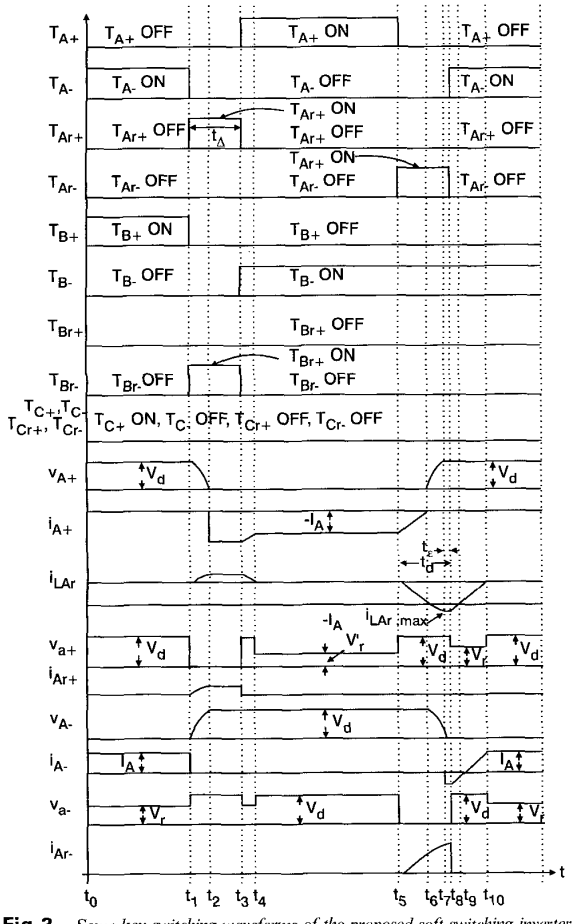


**Fig. 3** *Some key switching waveforms of the proposed soft-switching inverter within one switching period*

on-state or conduction-state depending on its current direction. The circuit operations and governing equations of the proposed inverter under various modes in these two states are described in detail in the Appendix (Section 8.1).

According to the analysis made in this Appendix, the soft-switching characteristics of all the switches and diodes employed in the proposed soft-switching inverter are summarised in Table 1. For the main switches and diodes, the ZVS and/or ZCS switchings are obtained, and the zero-voltage transitions of the main switches are successfully achieved. As for the auxiliary resonant branches, only hard switching at the switches' turn-off exists. However, since MOSFETS with much lower ratings can be employed for the switches, their switching losses are negligibly small owing to the very fast switching characteristics. This phenomenon can be observed from the simulated and measured results provided later. It follows that the proposed soft-switching inverter possesses much improved conversion efficiency compared with the conventional inverter.

**Table 1: Soft-switching characteristics of switches and diodes**

| Devices | | Soft-switching characteristics | |
|---|---|---|---|
| | | turn-on | turn-off |
| Main circuit | switches ($T_{A+}$–$T_{C-}$) | ZVS, ZCS | ZVS |
| | anti-parallel diodes ($D_{A+}$–$D_{C-}$) | ZVS | ZVS, ZCS |
| Auxiliary circuit | switches ($T_{Ar+}$–$T_{Cr-}$) | ZCS | none |
| | diodes ($D_{Ar+}$–$D_{Cr-}$) | ZCS | ZVS, ZCS |

## 3 Design of the proposed soft-switching inverter

### 3.1 Switching signal generating scheme

It is clear from the analysis made in the Appendix (Section 8.1) and the waveforms sketched in Fig. 3 that the proposed soft switchings can be successfully achieved by letting

the turn-on of the auxiliary switch intervene between the switchings of the upper and lower main switches of each leg. The turn-on interval of the auxiliary switch should satisfy the condition of eqn. 15. Generally, it is sufficient to let this turn-on interval be equal to the blanking time $t_\Delta$. This will significantly facilitate the implementation of the switching signal generating scheme. Accordingly, a switching signal generating scheme for realising the proposed PWM soft-switching control is shown in Fig. 4, which is easily obtained from the conventional PWM switching scheme by slight modification.

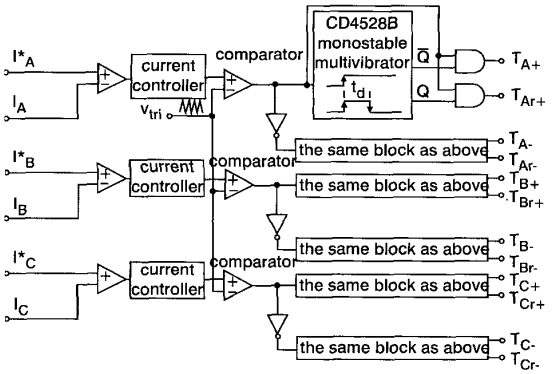


**Fig. 4** *Switching signal generating scheme of the proposed soft-switching inverter*

### 3.2 A systematic design procedure for an auxiliary resonant branch

***3.2.1 Observation:*** One can observe from eqns. 6 and 7 listed in the Appendix (Section 8.1) that the maximum values of $t_{12}$ and $I_{LAr,on}$ occurring at $I_A = 0$ in the on-state mode are

$$t_{12,max} = \pi/2(1/\omega_r) = \pi/2\sqrt{2L_rC_r} \qquad (1)$$

and

$$(I_{LAr,on})_{max} = V_d/Z_r \qquad (2)$$

respectively. Accordingly, the comparison between eqns. 1 and 2 and eqns. 13 and 14 (in the Appendix (Section 8.1)) indicates that $(t_{56} + t_{67}) > t_{12,max}$ and $|I_{LAr,max}| > (I_{LAr,on})_{max}$. It follows that the turn-on interval ($t_\Delta$) of the auxiliary switch and its current rating should be determined according to eqns. 13 and 14 in the conduction-state mode.

***3.2.2 Design procedure:*** The basic specifications of the inverter are given as:

maximum DC-link voltage = $V_{d,max}$

maximum induction motor line current = $I_{A,max}$

switching period $T_s = 1/f_s$

According to the governed equations derived in the previous Section and the waveforms sketched in Fig. 3, the circuit components of the auxiliary resonant branch can be systematically found according to the following procedure:

*Specify $t_d$ and $t_\varepsilon$*: Since $t_d = t_\Delta = t_{56} + t_{67} + t_\varepsilon$ from eqn. 15, if the delay time $t_d$ is specified too small there will be no sufficient time of $t_\varepsilon$ to let the circuit be normally operated. Conversely, if $t_d$ is too long, the PWM switching performance will be much deteriorated. Generally, $t_d$ can be specified to be $0.05(T_s)$ to $0.1(T_s)$, according to the typical value of the forward recovery time of the anti-parallel diode and the switching speed of the main switch, or it is also satisfactory to specify $t_d$ (= $t_\Delta$), according to the typical blanking time for the chosen main semiconductor switch.

*Determine the maximum resonant inductor current $I_{LAr,max}$*: It is clear from eqn. 13 and the waveforms sketched in Fig. 3 that $I_{LAr,max}$ should be greater than $I_{A,max}$ such that the main switch can be turned on with ZVS. Accordingly, it is convenient to let $I_{LAr,max} = xI_{A,max}$, $x > 1$. In practice, $1.3 < x < 1.5$ is a reasonable choice.

*Determination of $L_r$ and $C_r$*: From eqns. 13–15, the inductance of $L_r$ and capacitance of $C_r$ can be uniquely determined in sequence as follows:

$$L_r = \frac{V_{d,max}(t_d - t_\varepsilon)}{I_{A,max}\left(1 + (x-1)\frac{\pi}{2}\right)}$$

$$C_r = \frac{L_r}{2}\left[\frac{(x-1)I_{A,max}}{V_{d,max}}\right]^2 \qquad (3)$$

*Selection of auxiliary switches*: Since the conduction duty ratio of the auxiliary switch is very small, a small rating MOSFET can be employed. The details about the selection will be explained numerically in the following Section. Due to the high-speed switching characteristic of MOSFET and the possession of ZCS turn-on switching, very low switching losses of the auxiliary switches can be obtained.

Based on the design procedure described above and the given system ratings, the design of the circuit components of the proposed inverter is presented in the Appendix (Section 8.2).

## 4 Simulation and experimental results

Before performing the implementation, some Pspice simulations are made for a vector-controlled induction motor drive with an impressed current to check the validity of the analysis and design presented above. Under the maximum load current $I_{A,max}$ = 7.64A, the simulated waveforms of the designed soft-switching inverter with $f_s$ = 40kHz at on-state and conduction-state within a switching period are plotted in Fig. 5. The results show that $T_{A+}$ is operated in the on-state (modes 0 to 4) and $T_{A-}$ is operated in the conduction-state (modes 5 to 10) with the waveforms being similar to those predicted in Fig. 3. In addition, the values of the simulated variables are also all close to those derived.

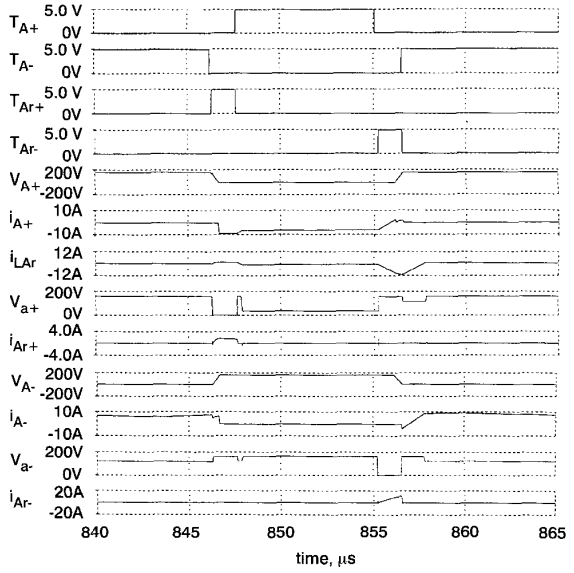


**Fig. 5** *Simulated voltage and current waveforms of the proposed soft-switching inverter within one switching period at $I_A$ = 7.64A*

Having tested the validity of the designed soft-switching scheme by simulation, the circuit of the designed inverter for driving the IFO induction motor drive, shown in Fig. 1, is implemented. The induction motor is mechanically coupled to a DC generator with a switched resistor as a dynamic load. The motor speed is operated at $\omega_{r0}$ = 1000rpm and $R_L = 27.8\Omega$. Figs. 6*a* and *b* show some measured waveforms of the main switch $T_{A-}$ and the auxiliary switch $T_{Ar-}$ of the designed soft-switching inverter. The results are very close to the predicted ones. One can observe from the results shown in Fig. 6 that, in addition to the main switch, the switching loss produced by the auxiliary switch is also very small. This confirms the comments made previously. For the same operating conditions, the measured waveforms of the inverter with a typical R-C snubber and conventional PWM hard switching are plotted in Fig. 7. Comparison between the results of Figs. 6 and 7 indicates that owing to the zero-voltage-transition by soft switching, the proposed inverter possesses much less switching power loss, turn-on d$v$/d$t$ and d$i$/d$t$ in the main switch.

The conversion efficiencies at three output powers under five switching frequencies are compared in Fig. 8.

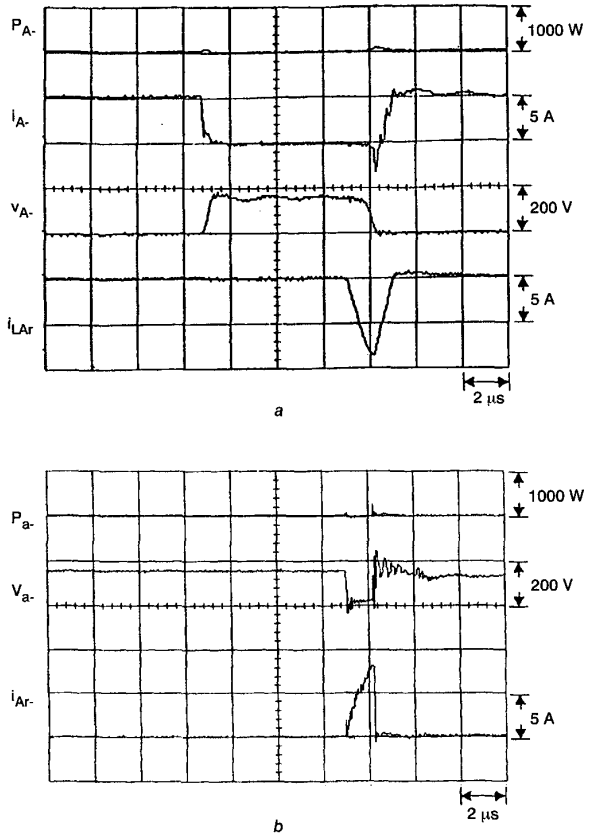


**Fig. 6** *Measured voltage, current and power waveforms of the designed soft-switching inverter at $\omega_{r0}$ = 1000rpm, $R_L = 27.8\Omega$*
*a $T_{A-}$*
*b $T_{Ar-}$*

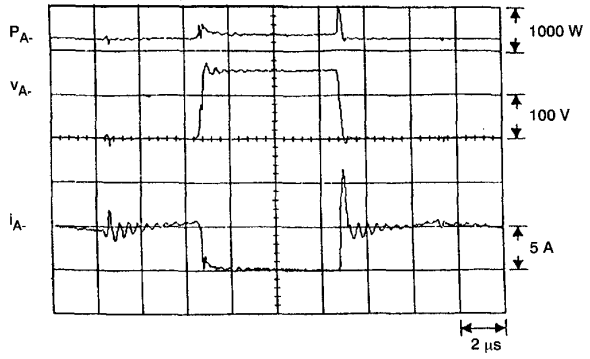


**Fig. 7** *Measured switching waveforms of $T_{A-}$ of the conventional hard-switching inverter at $\omega_{r0}$ = 1000rpm, $R_L = 27.8\Omega$*

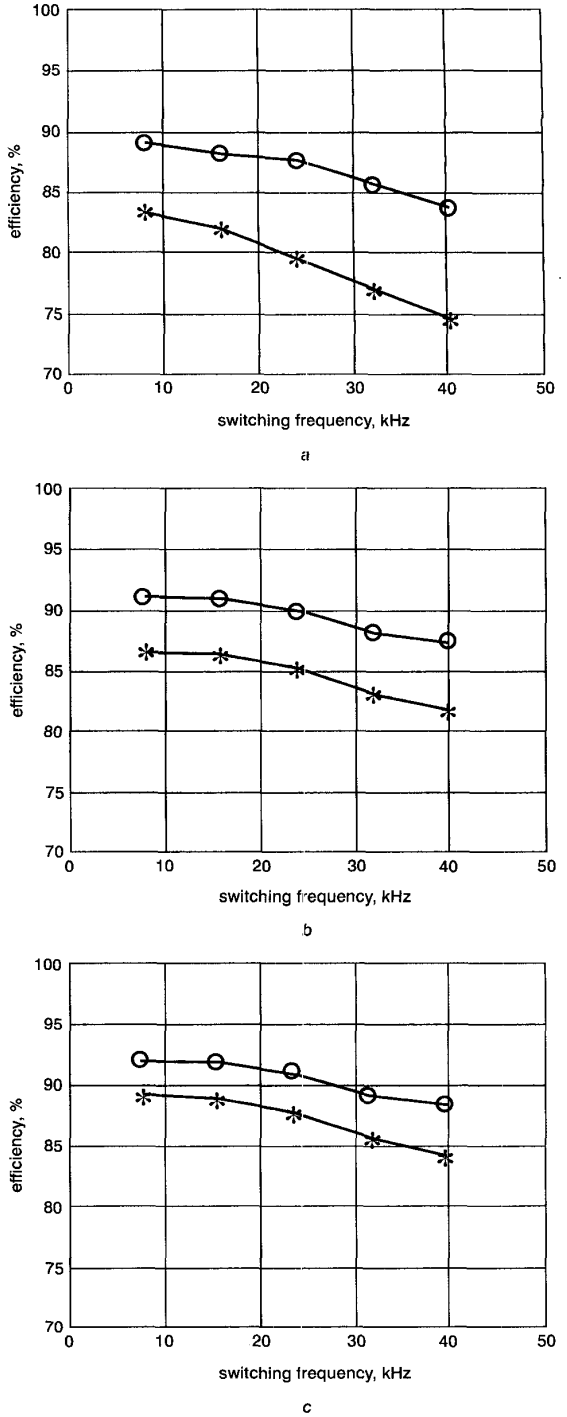


**Fig. 8** *Conversion efficiencies of the soft-switching inverter and hard-switching inverter at different switching frequencies*
*a $P_{out}$ = 200W*
*b $P_{out}$ = 430W*
*c $P_{out}$ = 800W*
○ soft switching
✳ hard switching

The efficiency of the inverter is measured by using the power meters placed at its input and output sides, and the efficiency is defined as $\eta \triangleq P_{out}/P_{in}$ ($P_{in}$ and $P_{out}$ denote the input and output powers of the inverter, respectively). Higher efficiencies yielded by the proposed inverter are clearly observed from the results shown in Fig. 8. The efficiency improvement at lighter load and higher switching frequency is more prominent, since the proportion of switching loss is larger.

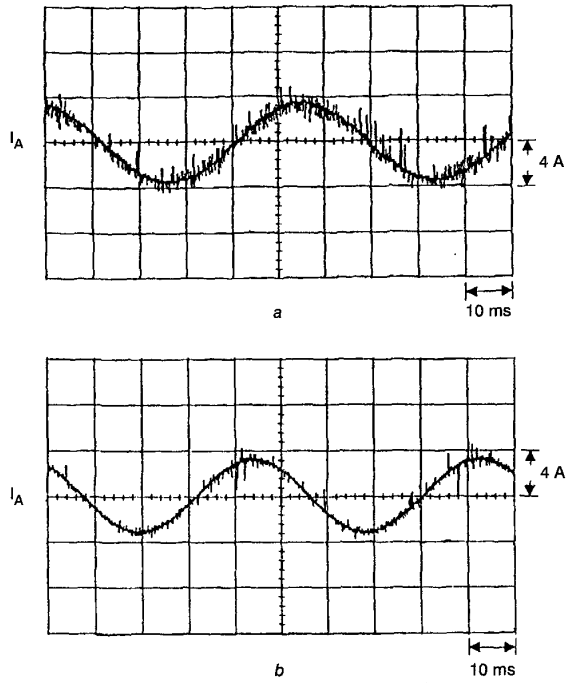


**Fig. 9** *Measured steady-state motor line current at $\omega_r^* = 1000$rpm, $R_L = 78.6\Omega$*
*a* Hard-switching inverter
*b* Soft-switching inverter

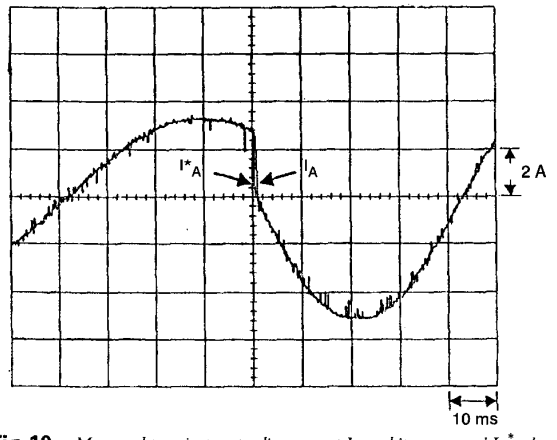


**Fig. 10** *Measured transient motor line current $I_A$ and its command $I_A^*$ when the motor is changed from ($\omega_r = 500$rpm, $R_L = 78.6\Omega$) to ($\omega_r = 1000$rpm, $R_L = 78.6\Omega$)*

Figs. 9*a* and *b* show the measured steady-state waveforms of the motor line currents $I_A$ by the hard- and soft-switching inverters at $\omega_r^* = 1000$rpm, $R_L = 78.6\Omega$, respectively. A large reduction in the high-frequency spikes by the proposed soft-switching inverter can be observed from the results. Finally, the measured transient motor line current $I_A$ and its command $I_A^*$ when the motor is changed from $\omega_r = 500$rpm, $R_L = 78.6\Omega$ to $\omega_r = 1000$rpm, $R_L = 78.6\Omega$ in step are plotted in Fig. 10. The smooth and fast-tracking current response is obtained by the designed inverter. The measured rotor speeds of the induction motor fed by the proposed soft-switching inverter due to the step command change $\omega_r^* = 1000\text{rpm} \rightarrow 1100\text{rpm}$ ($R_{L0} = 78.6\Omega$) and the load resistance change $R_{L0} = 78.6\Omega \rightarrow 27.8\Omega$ ($\omega_{r0} = 1000$rpm) are plotted in Figs. 11*a* and *b*. The results indicate that good current and speed control performances are obtained. It can be concluded from the results provided above that the proposed soft-switching inverter is easily obtained from the conventional one without sacrificing the current and speed responses of the motor drive. However, the switching losses, the conversion efficiencies and the switching stresses yielded by the inverter can be much reduced by using the proposed soft-switching technique.

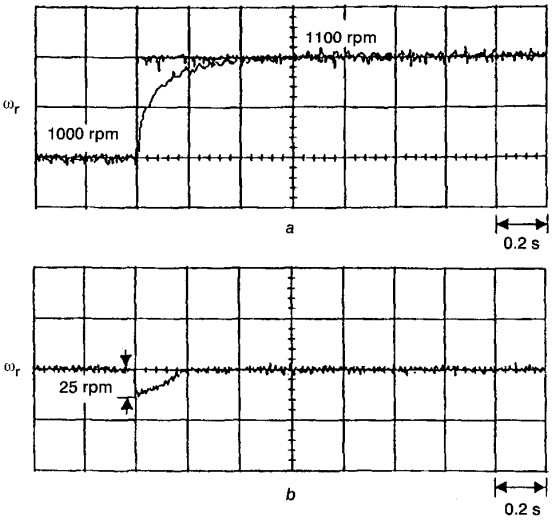


**Fig. 11** *Measured rotor speed dynamic responses*
a due to the step command change $\omega_r^* = 1000\text{rpm} \rightarrow 1100\text{rpm}$ ($R_{L0} = 78.6\Omega$)
b due to the load resistance change $R_{L0} = 78.6\Omega \rightarrow 27.8\Omega$ ($\omega_{r0} = 1000$rpm)

## 5 Conclusions

The design and implementation of a resonant snubber-based soft-switching inverter-fed indirect field-oriented induction motor drive are presented. The proposed soft-switching inverter is constructed from the conventional one by simply augmenting with auxiliary resonant branches, and the soft-switching is easily achieved by suitable switching of the auxiliary switch within the blanking time period of the main switches. The major advantage of the proposed inverter is that the switches in each inverter leg can be independently controlled, therefore the PWM switching control is very flexible. Having derived the governed equations in various operation modes, the quantitative design of the proposed soft-switching inverter is performed. The simulation and measured results demonstrate that good performances of the inverter and the induction motor drive are obtained through using the proposed soft-switching scheme.

## 6 Acknowledgment

This research was supported by the National Science Council, Taiwan, ROC, under grant #NSC-88-2213-E-007-084.

## 7 References


1 MOHAN, N., UNDELAND, T.M., and ROBBINS, W.P.: 'Power electronics: converter, application and design' (John Wiley & Sons, New York, 1995, 2nd edn.)
2 TRZYNADLOWSKI, A.M.: 'Introduction to modern power electronics' (John Wiley & Sons, New York, 1998)
3 DIVAN, D.M.: 'The resonant DC link converter — a new concept in static power conversion'. Conference Record of the IEEE IAS Annual Meeting, 1986, pp. 648–656
4 LORENZ, R.D., and DIVAN, D.M.: 'Dynamic analysis and experimental evaluation of delta modulators for field oriented AC machine current regulators'. Conference Record of the IEEE IAS Annual Meeting, 1987, pp. 196–201
5 DIVAN, D.M., and SKIBINSKI, G.: 'Zero switching loss inverters for high power applications'. Conference Record of the IEEE IAS Annual Meeting, 1987, pp. 627–634
6 DE DONCKER, R.W., and VENKATARAMANAN, G.: 'A new single phase AC to DC zero voltage soft switching converter', *IEEE Power Electron. Spec. Conf. Rec.*, 1990, pp. 206–211
7 HE, J., and MOHAN, N.: 'Parallel resonant DC link circuit — a novel zero switching loss topology with minimum voltage stresses', *IEEE Power Electron. Spec. Conf. Rec.*, 1989, pp. 1006–1012
8 MALESANI, L., TENTI, P., DIVAN, D.M., and TOIGO, V.: 'A synchronized resonant DC link converter for soft-switched PWM'. Conference Record of the IEEE IAS Annual Meeting, 1989, pp. 1037–1044
9 McMURRAY, W.: 'Resonant snubbers with auxiliary switches', *IEEE Trans. Ind. Appl.*, 1993, **IA–29**, (2), pp. 355–361
10 DE DONCKER, R.W., and LYONS, J.P.: 'The auxiliary resonant commutated pole converter'. Conference Record of the IEEE IAS Annual Meeting, 1990, pp. 1228–1235
11 VLATKOVIC, V., BOROJEVIC, D., and LEE, F.C.: 'A new zero-voltage transition, three-phase PWM rectifier/inverter circuit', *IEEE Power Electron. Spec. Conf. Rec.*, 1993, pp. 868–873
12 CUADROS, C., BOROJEVIC, D., GATARIC, S., MAO, H., and LEE, F.C.: 'Space vector modulated, zero-voltage transition three-phase to DC bidirectional converter', *IEEE Power Electron. Spec. Conf. Rec.*, 1994, pp. 16–23
13 LAI, J.S.: 'Resonant snubber-based soft-switching inverters for electric propulsion drives', *IEEE Trans. Ind. Appl.*, 1997, **IA–44**, (1), pp. 71–80
14 FINNEY, S.J., GREEN, T.C., and WILLIAMS, B.W.: 'Review of resonant link topologies for inverters', *IEE Proc. B, Electron. Power Appl.*, 1993, **B–140**, (2), pp. 103–114
15 PICKERT, V., and JOHNSON, C.M.: 'Three phase soft-switching voltage source converters for motor drives. Part 1: overview and analysis', *IEE Proc., Electr. Power Appl.*, 1999, **146**, (2), pp. 147–154
16 PICKERT, V., and JOHNSON, C.M.: 'Three phase soft-switching voltage source converters for motor drives. Part 2: fundamental limitations and critical assessment', *IEE Proc., Electr. Power Appl.*, 1999, **146**, (2), pp. 155–162
17 VAS, P.: 'Sensorless vector and direct torque control' (Oxford University Press, 1998)
18 NOVOTNY, D.W., and LIPO, T.A.: 'Vector control and dynamics of AC drives' (Clarendon Press, Oxford, 1996)


## 8 Appendix

### 8.1 Circuit operations and governing equations of the proposed inverter

*On-state*

*Mode 0 ($t_0 \sim t_1$)*: Referring to Fig. 3: assume that $T_{A-}$, $T_{B+}$ and $T_{C+}$ are conducting initially during $t_0 \le t \le t_1$, therefore $v_{A-} = v_{B+} = v_{C+} = 0$, and $v_{A+} = v_{B-} = v_{C-} = V_d$. The voltages across the auxiliary switches $T_{Ar+}$ and $T_{Ar-}$ are $v_{a+} = V_d$ and $v_{a-} = V_d C_{DAr-}/(C_{ar-} + C_{DAr-}) \triangleq V_r$, respectively, where $C_{ar-}$ and $C_{DAr-}$ (not explicitly shown in Fig. 12) denote the parasitic capacitances of $T_{Ar-}$ and $D_{Ar-}$. The current paths in this mode are shown in Fig. 12.

Mode 1 ($t_1 \sim t_2$): At $t = t_1$, the main switches $T_{A-}$ and $T_{B+}$ are turned off with ZVS, due to $v_{A-}(t_1) = v_{B+}(t_1) = 0$, and meanwhile the auxiliary switches $T_{Ar+}$ and $T_{Br-}$ (rather than the main switches $T_{A+}$ and $T_{B-}$) are turned on for a blanking time interval $t_\Delta$. This leads to the circuit configuration and current paths shown in Fig. 13. During this period, $v_{a+} = 0$ and $v_{a-} = V_d$. Through careful derivation, the resonant capacitor voltages and inductor current can be found to be

$$\begin{aligned} v_{CAr+}(t) &= v_{A+}(t) \\ &= V_d \cos\omega_r(t-t_1) - Z_r I_A \sin\omega_r(t-t_1) \\ &= \sqrt{V_d^2 + Z_r^2 I_A^2}\cos(\omega_r(t-t_1)+\phi) \\ v_{CAr-}(t) &= v_{A-}(t) \\ &= V_d - \sqrt{V_d^2 + Z_r^2 I_A^2}\cos(\omega_r(t-t_1)+\phi) \\ i_{LAr}(t) &= \sqrt{\frac{V_d^2}{Z_r^2} + I_A^2}[\sin(\omega_r(t-t_1)+\phi) - \sin\phi] \\ & t_1 \le t \le t_2 \end{aligned} \tag{4}$$

where

$$\omega_r \triangleq 1/\sqrt{2L_rC_r} \quad Z_r \triangleq \sqrt{\frac{L_r}{2C_r}} \quad \phi \triangleq \tan^{-1}\frac{Z_r I_A}{V_d} \tag{5}$$

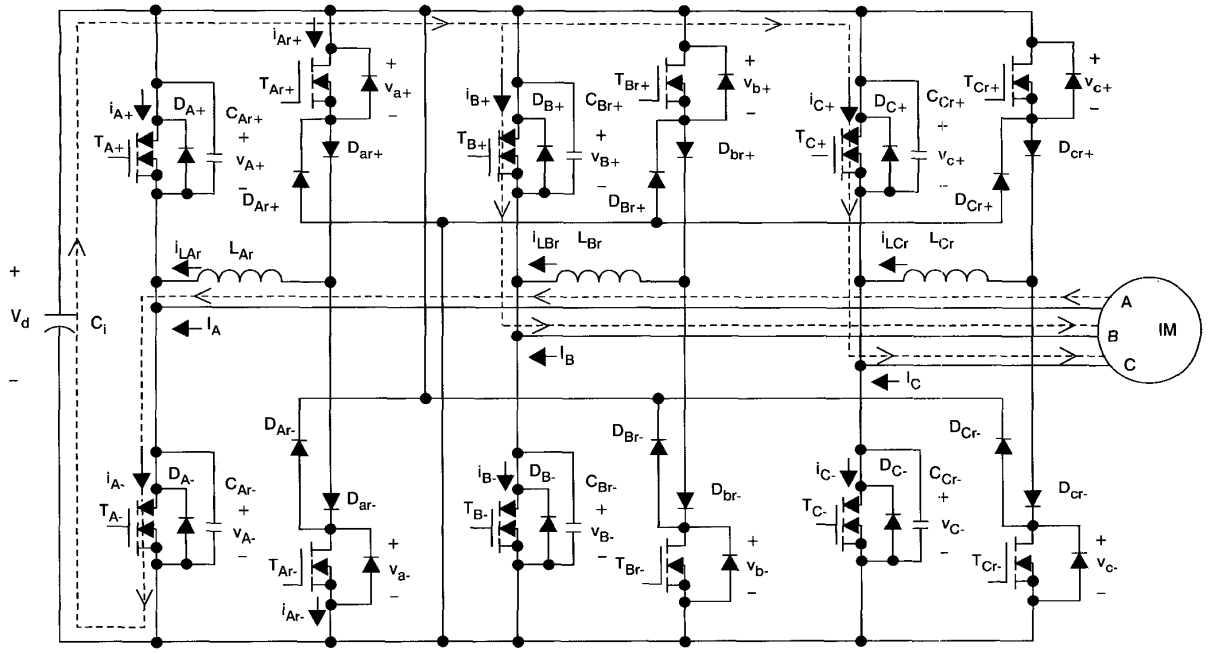


**Fig. 12** *Circuit configuration and current paths of mode 0*

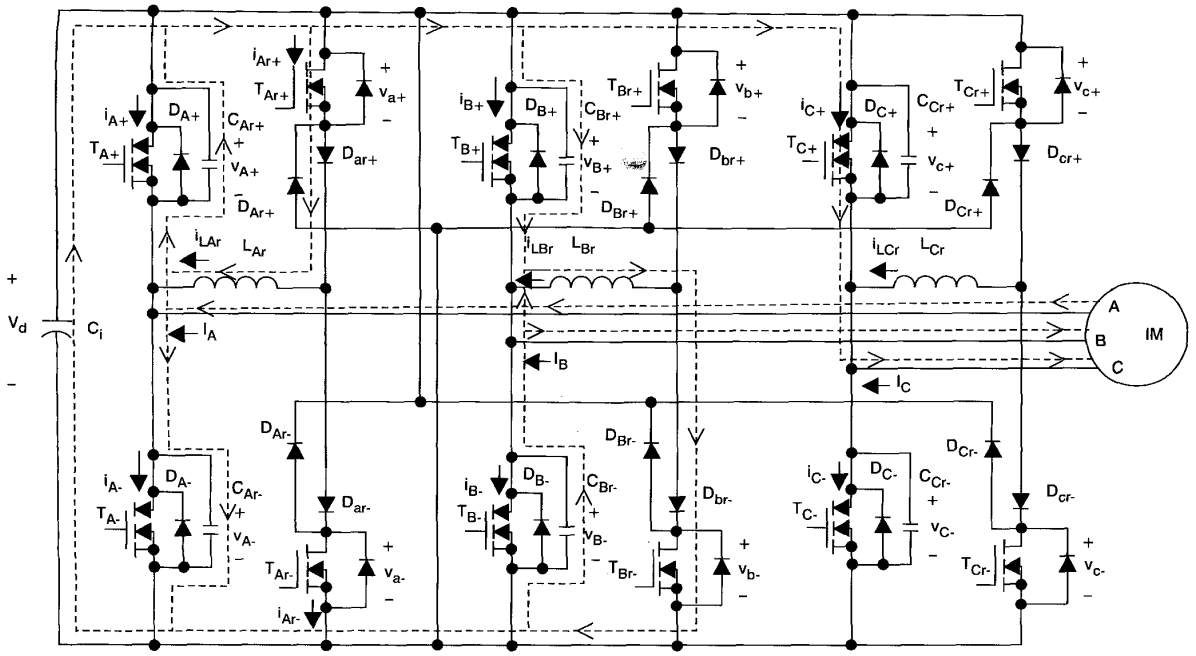


**Fig. 13** *Circuit configuration and current paths of mode 1*

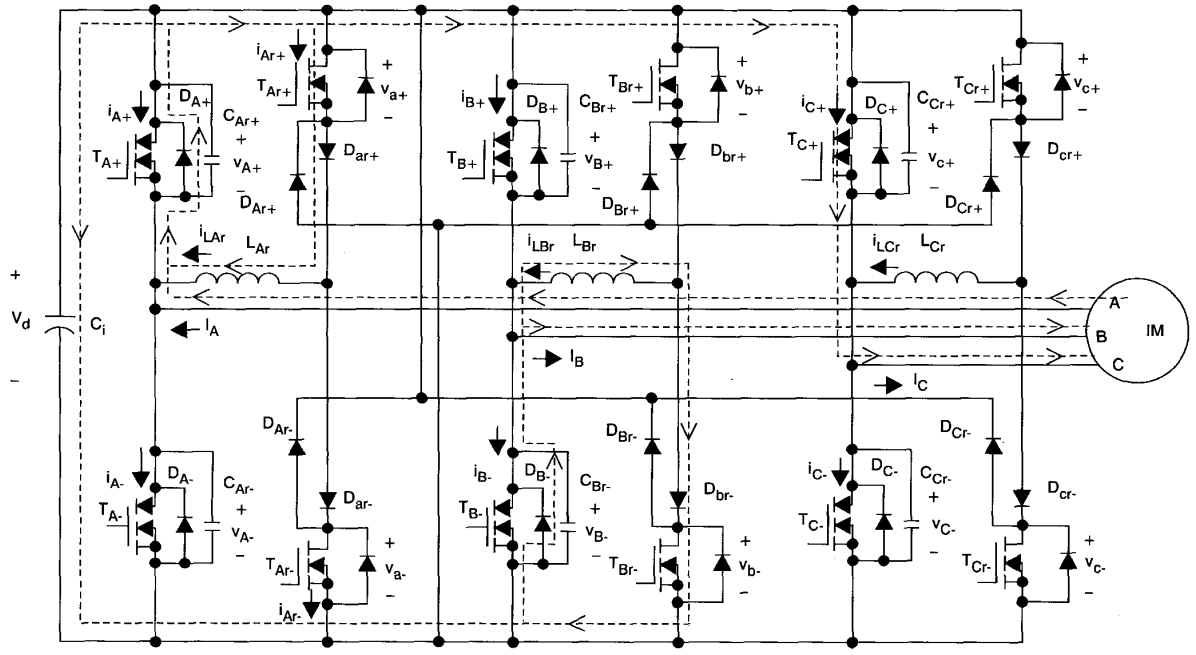


**Fig. 14** *Circuit configuration and current paths of mode 2*

At $t = t_2$, $C_{Ar-}$ is charged to $v_{CAr-}(t_2) = v_{A-}(t_2) = V_d$, and $C_{Ar+}$ is discharged to $v_{CAr+}(t_2) = v_{A+}(t_2) = 0$. This leads to the conduction of $D_{A+}$ with ZVS. From eqns. 4 and 5, one can find the time interval and the final value of the resonant inductor current of this mode as

$$t_{12} \triangleq t_2 - t_1 = \frac{1}{\omega_r}\left(\frac{\pi}{2} - \phi\right) \tag{6}$$

$$i_{LAr}(t_2) \triangleq I_{LAr,on} = \sqrt{\frac{V_d^2}{Z_r^2} + I_A^2}(1 - \sin\phi) \tag{7}$$

*Mode 2 ($t_2 \sim t_3$)*: As the anti-parallel diode $D_{A+}$ conducts at $t = t_2$, the circuit enters into mode 2 as shown in Fig. 14 with its initial resonant inductor current $i_{LAr}(t_2) = I_{LAr,on}$ and the main switch current $i_{A+}(t_2) = -I_A - I_{LAr,on}$. This mode ends at $t = t_3$ with the time interval of $t_{23} = t_3 - t_2 = t_\Delta - t_{12}$. Due to a very small resistance of the flywheeling path formed by $T_{Ar+}$, $D_{ar+}$, $L_{Ar}$ and $D_{A+}$, both $i_{LAr}$ and $i_{A+}$ keep nearly constant during this short interval mode. In this mode, $v_{a+} = 0$ and $v_{a-} = V_d$.

*Mode 3 ($t_3 \sim t_4$)*: At $t = t_3$, the auxiliary switch $T_{Ar+}$ is turned off and the main switch $T_{A+}$ is turned on simultaneously. The freewheeling diode $D_{Ar+}$ conducts, and $T_{A+}$ is

in an on-state (owing to $i_{A+} < 0$). This leads to the circuit configuration and current paths indicated in Fig. 15. The main switch $T_{A-}$ voltage is clamped at $V_d$, the resonant inductor current $i_{LAr}$ decreases linearly from $I_{LAr,on}$ and the main switch current $i_{A+}$ increases linearly from $(-I_A - I_{LAr,on})$. In this mode, the energy stored in the resonant inductor is transferred back into the DC source. At $t = t_4$ this mode ends at which $i_{LAr}(t_4) = 0$ and $i_{A+}(t_4) = -I_A$. The time interval of this mode can be found as

$$t_{34} \triangleq t_4 - t_3 = \frac{L_r}{V_d} I_{LAr,on} \tag{8}$$

During this period, $v_{a+} = V_d$ and $v_{a-} = V_r$.

*Mode 4 ($t_4 \sim t_5$)*: At $t = t_4$, $i_{LAr}(t_4) = 0$, $D_{Ar+}$ turns off with ZCS, and this leads to the circuit configuration of Fig. 16 with $i_{A+} = -I_A$ steadily. The voltages are $v_{a+} = V_d - V_r \triangleq V_r'$ and $v_{a-} = V_d$ in this mode. The switching operation from $T_{A-}$ (conduction-state) to $T_{A+}$ (on-state, $D_{A+}$ conducting) is completed.

Conduction-state

*Mode 5 ($t_5 \sim t_6$)*: Initially, $T_{A+}$, $T_{B-}$ and $T_{C+}$ are on at $t = t_5$, accordingly, $v_{A+}(t_5) = 0$, $v_{A-}(t_5) = V_d$ and $i_{LAr}(t_5) = 0$. Referring to Fig. 3: at $t = t_5$, the main switch $T_{A+}$ is turned off with ZVS, due to $v_{A+}(t_5) = 0$, and the auxiliary switch $T_{Ar-}$, rather than the main switch $T_{A-}$, is turned on. This

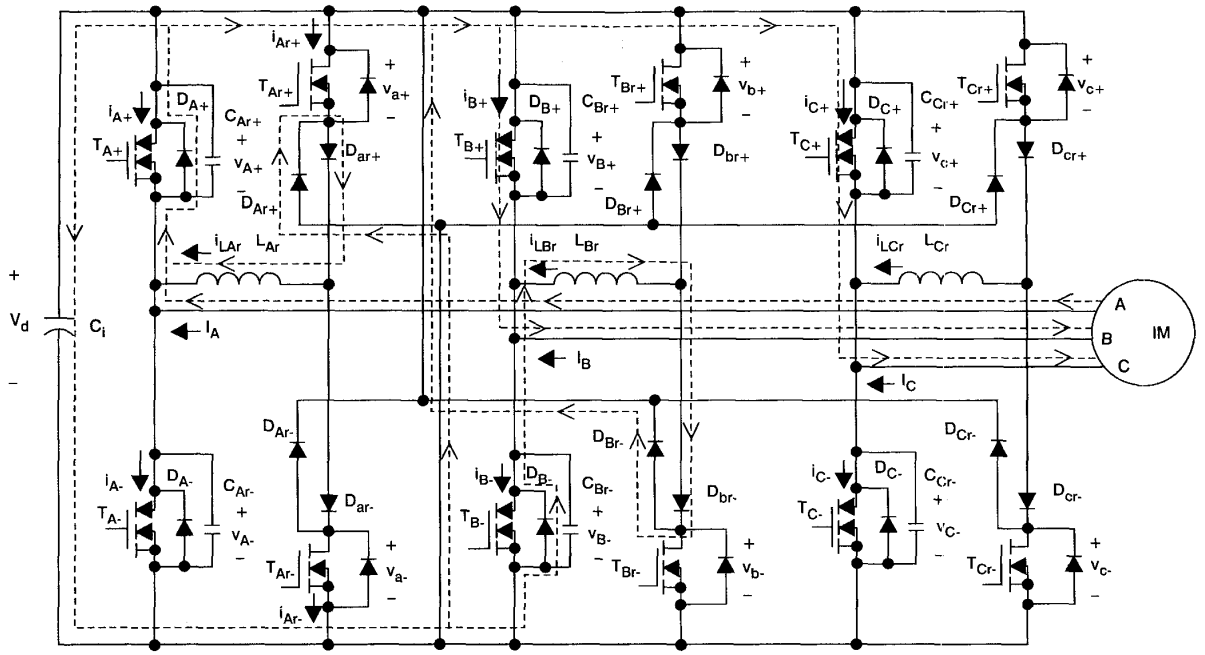


**Fig. 15** *Circuit configuration and current paths of mode 3*

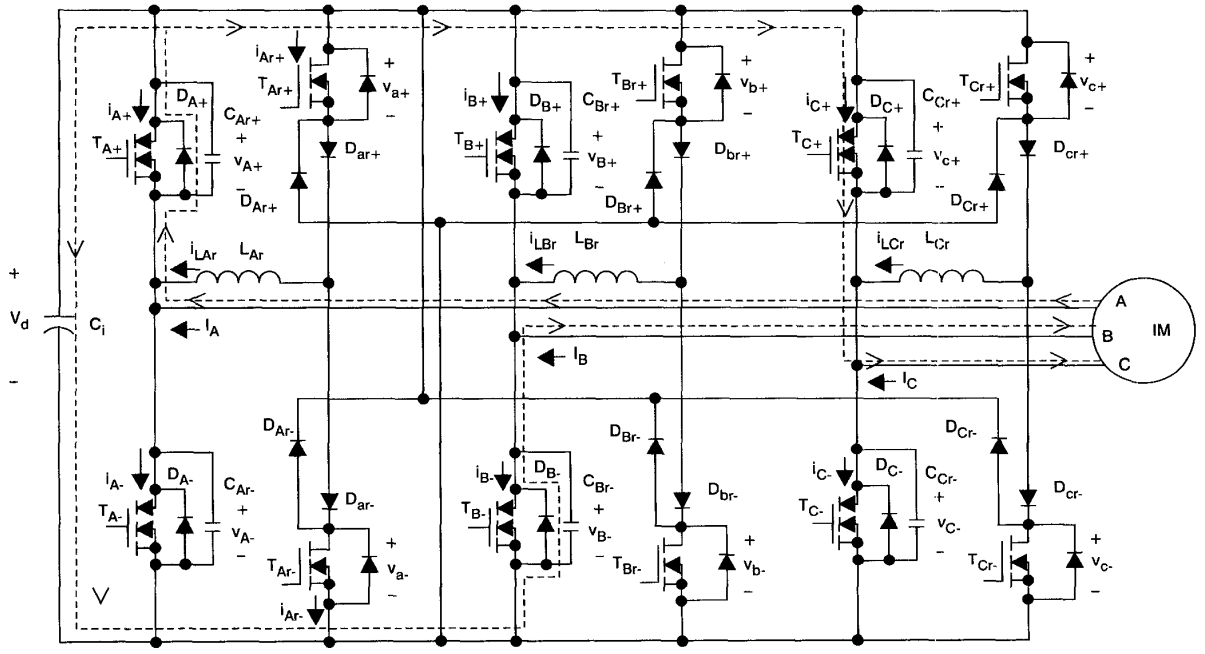


**Fig. 16** *Circuit configuration and current paths of mode 4*

leads to the circuit configuration shown in Fig. 17. The resonant inductor current can be found as

$$i_{LAr}(t) = \frac{-V_d}{L_r}(t - t_5) \qquad t_5 \le t \le t_6 \qquad (9)$$

The resonant inductor current $i_{LAr} = -i_{Ar-}$ increases linearly in the negative direction until it reaches $-I_A$ at $t_6$ where $D_{A+}$ is turned off with ZCS. This mode ends at $t = t_6$ with the time interval found from eqn. 9:

$$t_{56} \triangleq t_6 - t_5 = \frac{L_r I_A}{V_d} \qquad (10)$$

In this interval, $v_{a+} = V_d$ and $v_{a-} = 0$.

*Mode 6 ($t_6 \sim t_7$)*: After the turn-off of $D_{A+}$ at $t = t_6$, the resonant circuit is formed by $L_{Ar}$, $C_{Ar+}$, $C_{Ar-}$, $D_{ar-}$ and $T_{Ar-}$, as shown in Fig. 18 with the initial condition $i_{LAr}(t_6) = -I_A$. The resonant inductor current and the capacitor voltages are found to be

$$\begin{aligned} v_{A-}(t) &= V_d \cos\omega_r(t - t_6) \\ v_{A+}(t) &= V_d - V_d \cos\omega_r(t - t_6) \\ i_{LAr}(t) &= -I_A - \frac{V_d}{Z_r}\sin\omega_r(t - t_6) \quad t_6 \le t \le t_7 \end{aligned} \qquad (11)$$

The resonant inductor current $i_{LAr}$ continues to increase in

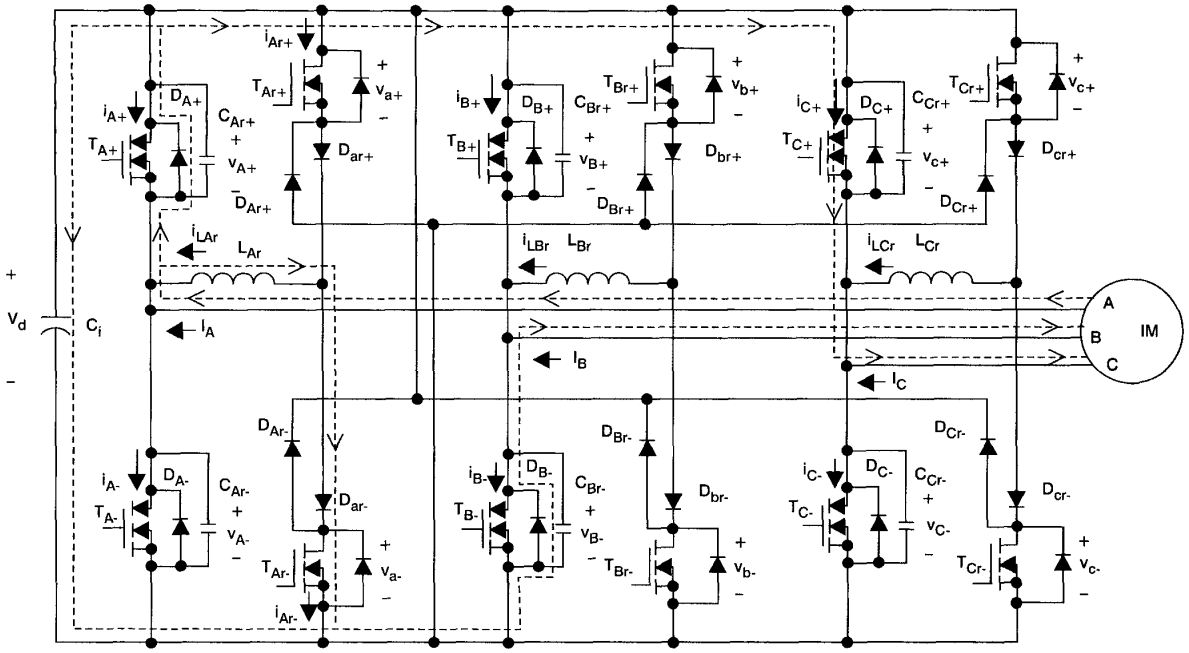


**Fig. 17** *Circuit configuration and current paths of mode 5*

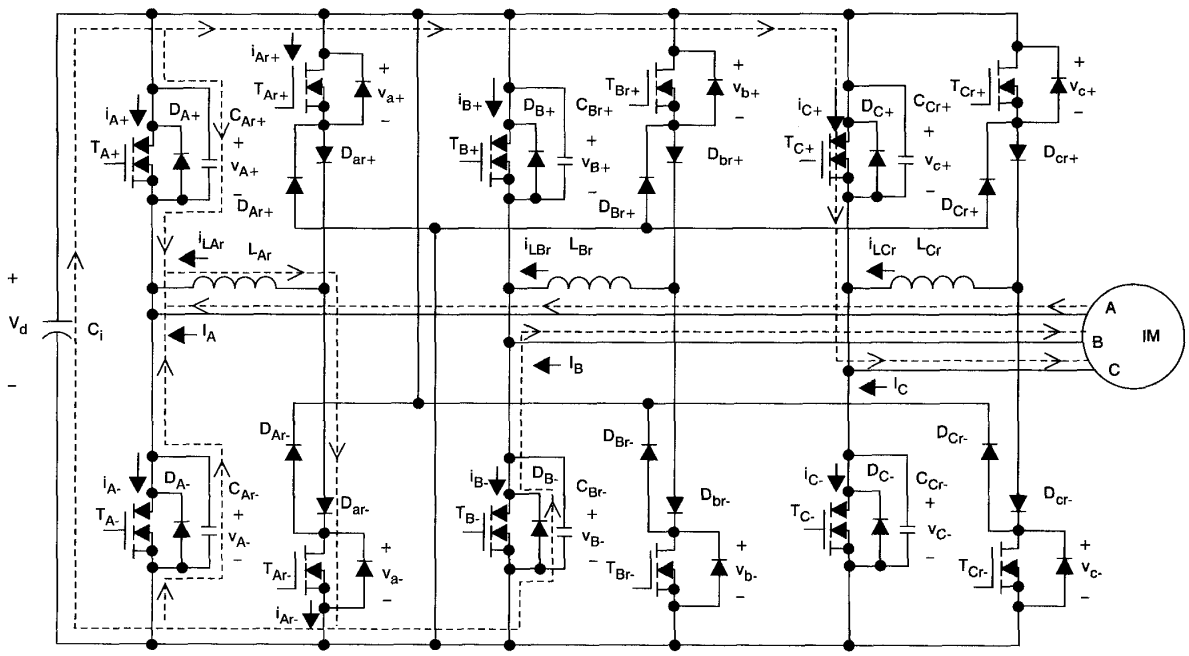


**Fig. 18** *Circuit configuration and current paths of mode 6*

the negative direction. During this interval, $C_{Ar-}$ is discharged to zero and $C_{Ar+}$ is charged to $V_d$ at $t_7$ where $D_{A-}$ conducts with ZVS. From eqn. 11, one can find the time interval of this mode and the maximum resonant inductor current as

$$t_{67} \triangleq t_7 - t_6 = \frac{\pi}{2}\sqrt{2L_rC_r} \tag{12}$$

$$I_{LAr,max} \triangleq i_{LAr}(t_7) = -I_A - \frac{V_d}{Z_r} \tag{13}$$

During this interval, $v_{a+} = V_d$ and $v_{a-} = 0$.

*Mode 7 ($t_7 \sim t_8$)*: As $C_{Ar-}$ is discharged to zero at $t = t_7$, the anti-parallel diode $D_{A-}$ turns on with ZVS with initial current $i_{A-} = -V_d/Z_r$. It is clear from Figs. 3 and 19 that the turn-on of the main switch $T_{A-}$ will be ZVS if its switching control signal is applied at a time instant after $t_7$. From eqns. 10 and 12, one can find the delay time $t_d$ for turning on the main switch $T_{A-}$ with ZVS should fulfil the following condition:

$$t_d > t_{56} + t_{67} = \frac{L_rI_A}{V_d} + \frac{\pi}{2}\sqrt{2L_rC_r} \tag{14}$$

In the proposed switching scheme, it is satisfactory to let

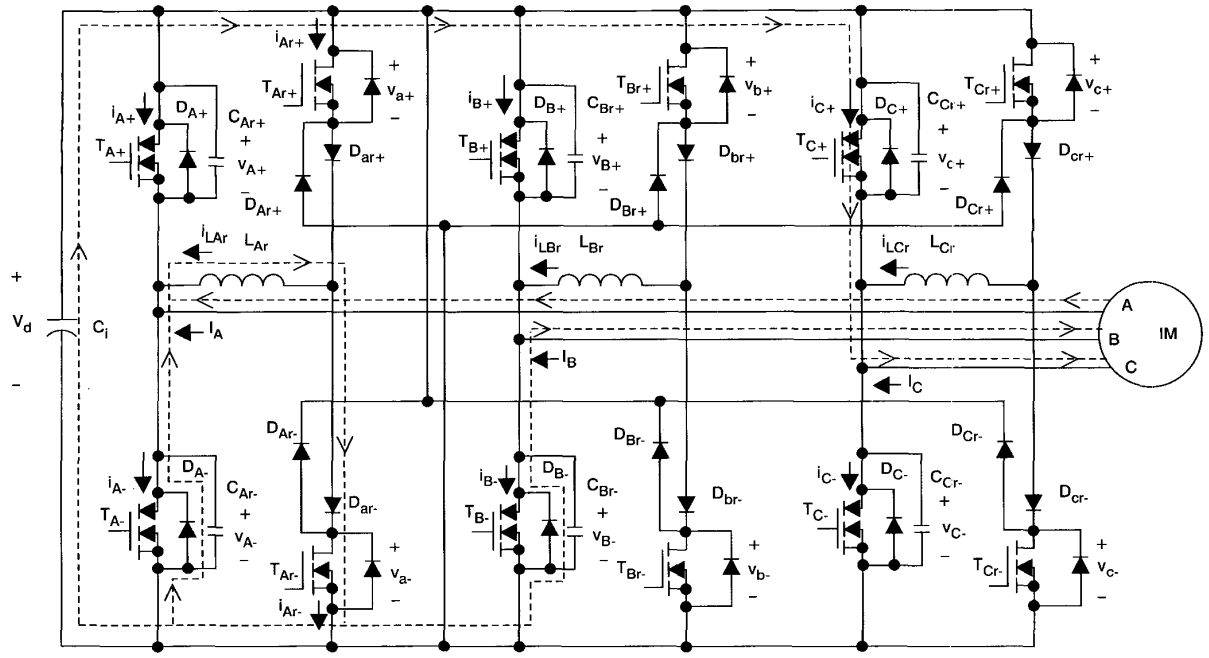


**Fig. 19** *Circuit configuration and current paths of mode 7*

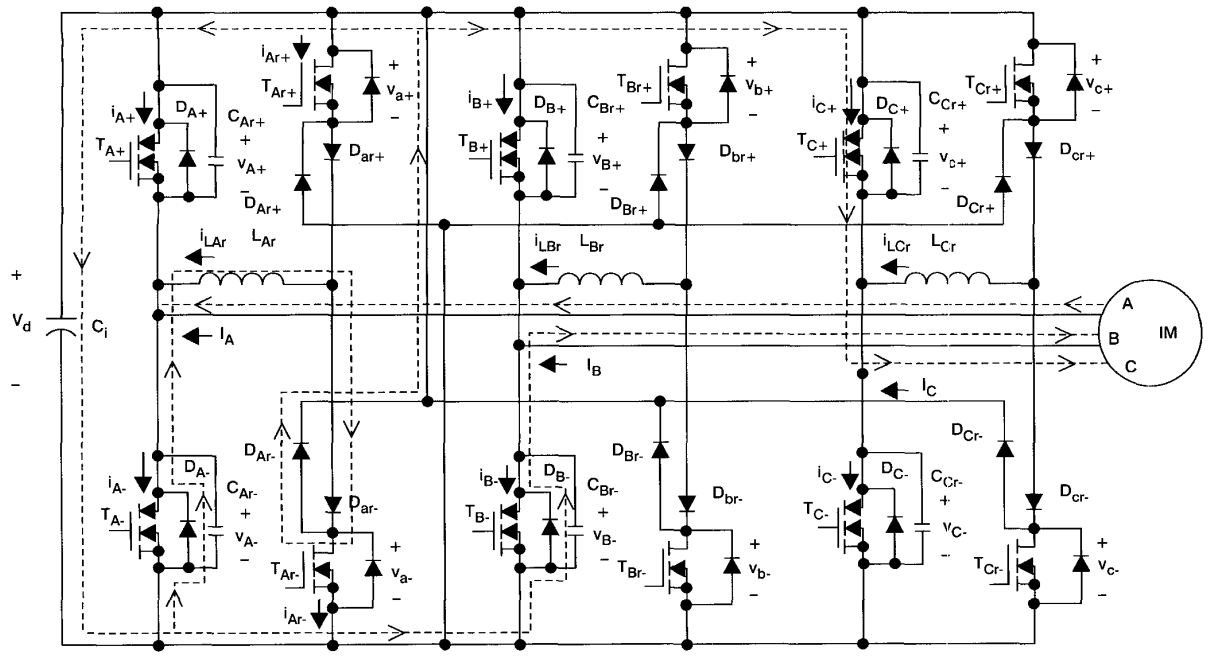


**Fig. 20** *Circuit configuration and current paths of mode 8*

$t_d = t_\Delta$. Considering the time interval $t_\varepsilon$ within which $D_{A-}$ enters the conduction state completely through the forward recovery process; the delay time $t_d$ can be set as

$$t_d = t_\Delta \triangleq t_{56} + t_{67} + t_\varepsilon \tag{15}$$

The voltages $v_{a+}$ and $v_{a-}$ are kept at the same values as those in mode 6.

*Mode 8 ($t_8 \sim t_9$)*: At $t = t_8$, the auxiliary switch $T_{Ar-}$ is turned off and the main switch $T_{A-}$ is turned on. Initially, $i_{A-}$ is negative, so $T_{A-}$ is in the on-state and the freewheeling diode $D_{A-}$ conducts. The circuit configuration and current paths are shown in Fig. 20. It can be found that $i_{LAr}$ increased linearly toward $-I_A$ at $t = t_9$, i.e. $i_{LAr}(t_9) = -I_A$ and $i_{A-}(t_9) = 0$. At $t = t_9$, this mode ends and $T_{A-}$ turns on with ZVS. One can find the time interval of this mode from

$$t_{89} \triangleq t_9 - t_8 = \frac{L_r}{Z_r} \tag{16}$$

During this interval, the $v_{a-}$ voltage is charged from 0 to $V_d$, and $v_{a+}$ is discharged from $V_d$ to $V_r$.

*Mode 9 ($t_9 \sim t_{10}$)*: The main switch $T_{A-}$ enters the conduction state after $t_9$ due to $i_{A-} > 0$. The circuit configuration and current paths are shown as Fig. 21. The main switch current $i_{A-}$ increases linearly from zero and the inductor current $i_{LAr}$ increases linearly from $-I_A$. At $t = t_{10}$, $i_{A-}(t_{10}) = I_A$ and $i_{LAr}(t_{10}) = 0$, so that $D_{Ar-}$ turns off with ZCS. The

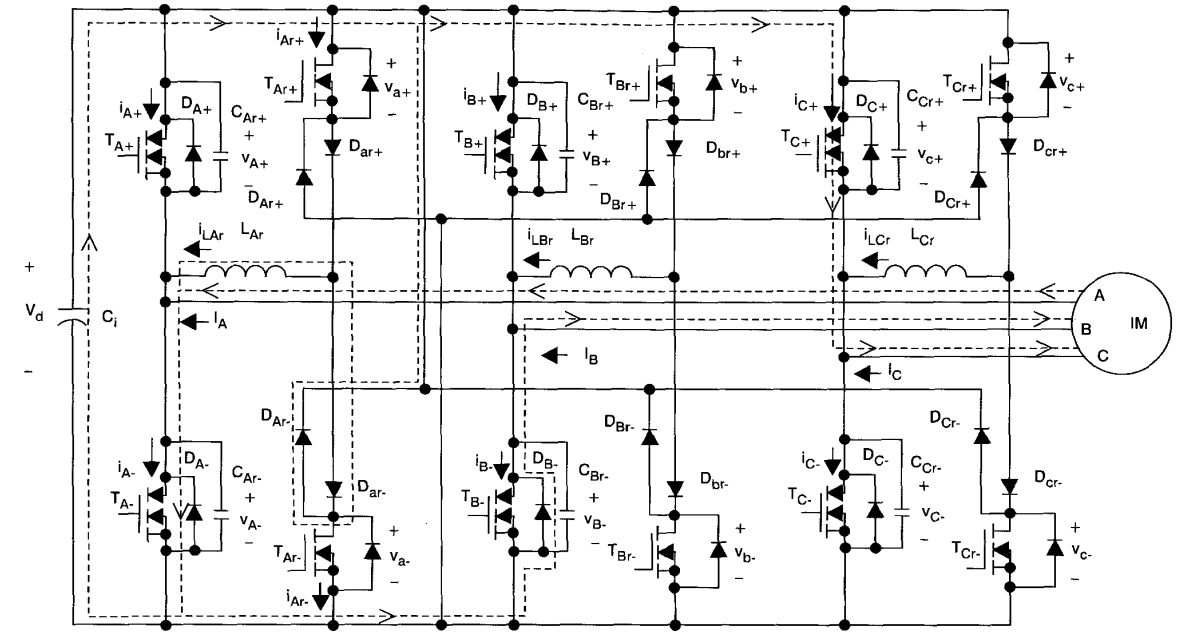


**Fig. 21** *Circuit configuration and current paths of mode 9*

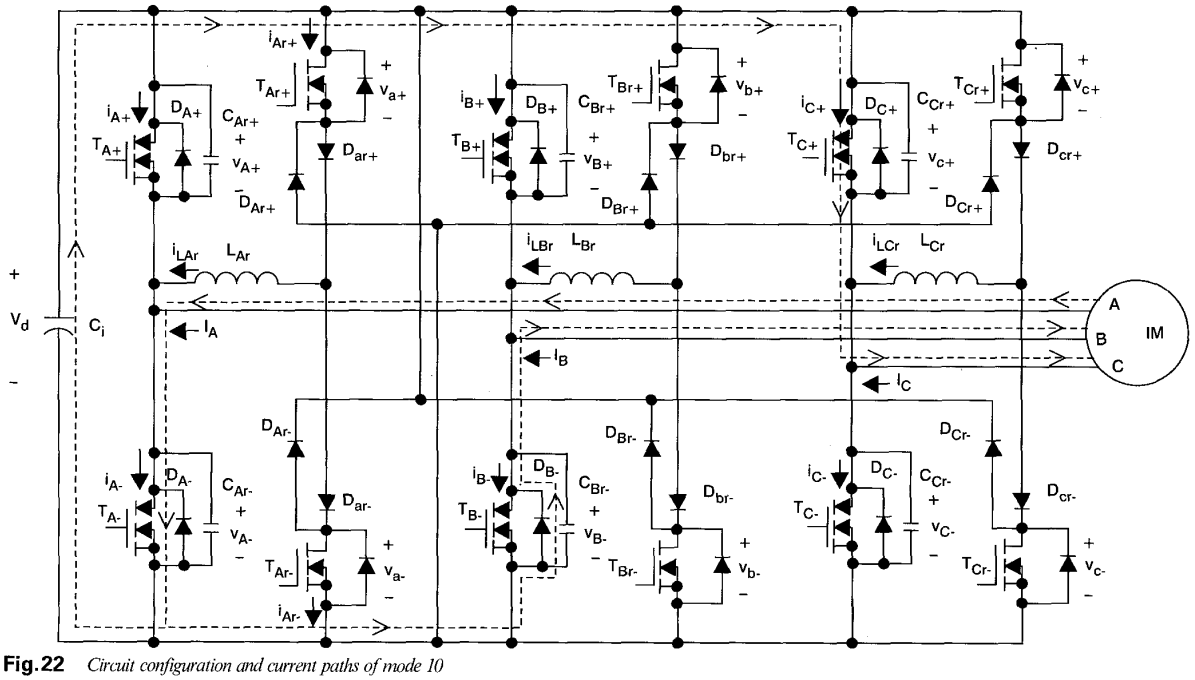


**Fig. 22** *Circuit configuration and current paths of mode 10*

time interval of this mode is

$$t_{9,10} \triangleq t_{10} - t_9 = \frac{L_r I_A}{V_d} \tag{17}$$

During this mode, both $v_{a+}$ and $v_{a-}$ are kept at the same values as those in mode 8.

*Mode 10 ($t_{10}$ ~)*: After the turn-off of $D_{Ar-}$ at $t \geq t_{10}$, the circuit configuration becomes that shown in Fig. 22. $T_{A-}$ conducts the load current totally, and one cycle of the switching operation from $T_{A+}$ ON (on-state) to $T_{A-}$ ON (conduction-state) is completed. The soft-switching is achieved by simply arranging the turn-on of the auxiliary switch $T_{Ar-}$ within the blanking time interval.

### 8.2 Design of circuit components

The ratings of the proposed soft-switching inverter driving a three-phase 800W, 120V, 5.4A, 2000rpm induction motor are listed as follows:

$$V_{d,max} = 160\,\text{V} \qquad I_{A,max} = 5.4\sqrt{2} = 7.64\,\text{A}$$
$$f_s = 40\,\text{kHz} \quad (T_s = 25\,\mu\text{s}) \tag{18}$$

The components of the inverter shown in Fig. 2 are designed according to the previous analysis to be:

*Main switches*: According to the voltage and current ratings listed in eqn. 18, the IGBT module is chosen: CM20TF-12H (20A/600V) (manufactured by Mitsubishi Electric).

*Resonant auxiliary branch*: By specifying $I_{LAr,max} = 1.4I_{A,max} = 10.7\text{A}$, $t_d = 0.06T_s$ and $t_\varepsilon = 0.005T_s$ (i.e. $t_\Delta = 1.5\mu\text{s}$, which is a reasonable blanking time for the chosen IGBT of the main switch) the values of the resonant inductor and the capacitor can be found from eqn. 3 to be $L_r = 17.7\mu\text{H}$ and $C_r = 3\text{nF}$. The fast diode RURP820 (manufactured by Harris Semiconductors) is chosen for all the diodes in the resonant branches.

Finally, according to the given data, one can find that $(I_{LAr,on})_{max} = 2.95\text{A}$ ($< I_{LAr,max} = 10.7\text{A}$) and $t_{12,max} = \pi/2\sqrt{2L_rC_r} = 0.512\mu\text{s}$ ($< t_d = t_\Delta = 0.05T_s = 1.5\mu\text{s}$). This confirms the observation made above. Therefore the $L_r$ and $C_r$ designed at the worst case, $I_A = I_{A,max}$ in the conduction state are satisfactory for any other load conditions.

From Fig. 3 and the data given above, the worst auxiliary switch current can be regarded as a periodic pulse with a duty ratio of 6% and an amplitude of 10.7A. According to the MOSFET data book, IRF840 having the following parameters may be a tentative candidate:

$V_{DS} = 500\text{V}$, $I_D = 8\text{A}$

$R_{DS(on)} = 1.92\Omega$ at $I_D = 10.7\text{A}$ and the maximum junction temperature $T_j = 150°\text{C}$

$R_{\theta JC} = 0.1°\text{C/W}$ when the duty ratio = 6% and the pulse width < 10μs

The single-pulse power dissipation of the assumed current waveform can be calculated as

$$P_{DM} = 10.7^2 \times 1.92 = 219.8\,\text{W}$$

If the case temperature is reasonably assumed to be 65°C, the junction temperature in this case can be estimated to be

$$T_j = 65 + 219.8 \times 0.1 = 86.98°\text{C} \ (< 150°\text{C})$$

It follows that IRF840 is suited to be an auxiliary switch in the designed soft-switching scheme.